

MicroNAS: Memory and Latency Constrained Hardware-Aware Neural Architecture Search for Time Series Classification on Microcontrollers

TOBIAS KING, Karlsruhe Institute of Technology, Germany

YEXU ZHOU, Karlsruhe Institute of Technology, Germany

TOBIAS RÖDDIGER, Karlsruhe Institute of Technology, Germany

MICHAEL BEIGL, Karlsruhe Institute of Technology, Germany

This paper presents MicroNAS, a system designed to automatically search and generate neural network architectures capable of classifying time series data on resource-constrained microcontrollers (MCUs) and generating standard tf-lite ML models. MicroNAS takes into account user-defined constraints on execution latency and peak memory consumption on a target MCU. This approach ensures that the resulting neural network architectures are optimised for the specific constraints and requirements of the MCU on which they are implemented. To achieve this, MicroNAS uses a look-up table estimation approach for accurate execution latency calculations, with a minimum error of only $\pm 1.02\text{ms}$. This accurate latency estimation on MCUs sets it apart from other hardware-aware neural architecture search (HW-NAS) methods that use less accurate estimation techniques. Finally, MicroNAS delivers performance close to that of state-of-the-art models running on desktop computers, achieving high classification accuracies on recognised datasets (93.93% on UCI-HAR and 96.33% on SkodaR) while running on a Cortex-M4 MCU.

CCS Concepts: • **Computing methodologies** → **Machine learning**; **Search methodologies**.

Additional Key Words and Phrases: Time Series, Classification, Hardware Aware Neural Architecture Search, Microcontrollers, Differentiable Neural Architecture Search

ACM Reference Format:

Tobias King, Yexu Zhou, Tobias Röddiger, and Michael Beigl. 2023. MicroNAS: Memory and Latency Constrained Hardware-Aware Neural Architecture Search for Time Series Classification on Microcontrollers. In . ACM, New York, NY, USA, 20 pages. <https://doi.org/XXXXXXX.XXXXXXX>

1 INTRODUCTION

Microcontrollers are small, low-power computing systems that can be found in a wide range of devices, including medical equipment, consumer electronics, wearables and much more. Deploying machine learning models directly on microcontrollers enables applications such as predictive maintenance [9], human activity recognition [34] or health monitoring [3] to be always available without network connectivity while ensuring privacy [11]. Many of these devices utilize sensors, such as GPS, accelerometers, gyroscopes and more which generate time series data [37].

The combination of sensors and processors in close proximity creates the opportunity to run machine learning algorithms close to the sensors, which allows these devices to operate in privacy-critical or real-time systems, in which data can or should not be sent to a server for processing and edge computing is the only viable solution. However, MCUs are equipped with constrained hardware, especially memory (SRAM) and processing power. An ARM Cortex-M4 microcontroller may only have 64 kB of SRAM and a CPU that clocks at only 64 MHz. With this hardware, it is impossible

Permission to make digital or hard copies of all or part of this work for personal or classroom use is granted without fee provided that copies are not made or distributed for profit or commercial advantage and that copies bear this notice and the full citation on the first page. Copyrights for components of this work owned by others than ACM must be honored. Abstracting with credit is permitted. To copy otherwise, or republish, to post on servers or to redistribute to lists, requires prior specific permission and/or a fee. Request permissions from permissions@acm.org.

© 2023 Association for Computing Machinery.

Manuscript submitted to ACM

to run state-of-the-art time series classification architectures such as InceptionTime [16] or DeepConvLSTM [31] which are designed for desktop computers. To obtain the best performance in these resource-constraint environments, architectures must be specialized for both concrete datasets and MCUs. Creating such a specialized architecture is often done by domain experts with knowledge in the field of machine learning which is a time-consuming and error-prone process, which often yields suboptimal results [29]. As an alternative, Hardware Aware Neural Architecture Search (HW-NAS) [7] could be used to automatically find architectures that obey to user-defined limits on the peak memory consumption and execution latency when running on the target device. However, existing HW-NAS systems are not suitable for time series classification [22, 39, 40, 42] and in addition, commonly utilize imprecise estimates to compute the expected execution latency of architectures [22, 39, 42].

To close this gap, we introduce MicroNAS, a HW-NAS system to find suitable neural network architectures for time series classification on microcontrollers. While doing so, MicroNAS respects user-imposed limits on the SRAM memory consumption and execution latency on a target MCU. To precisely calculate the execution latency of architectures in the search space, we utilize a lookup table approach where we store the execution latency of each operator in the search space. We show how to combine the lookup table latency calculation with masked convolutions [39] to support searching for the number of filters in a convolution which results in a fine granular search space. To support different datasets without having to adjust system parameters, we introduce a novel search space consisting of two types of cells whose architectures can be learned. The newly introduced Time-Reduce cell aggregates information in the temporal domain and reduces the length of the time series while the Sensor-Fusion cell allows for cross-channel interaction. These cells are automatically stacked according to the used dataset based on its window-size and its number of sensors.

In sum, our paper makes the following three contributions:

- (1) MicroNAS; the **first hardware-aware neural architecture search (HW-NAS) system for time series classification tasks on embedded microcontrollers** with the following unique properties:
 - (a) *a first-of-its-kind NAS search space specifically designed for time series classification on microcontrollers;*
 - (b) *the use of dynamic convolutions coupled with a lookup table approach for an efficient architecture search.*
 - (c) *support for datasets with various input dimensions, with varying number of sensors and window sizes, by introducing two searchable cells that summarize time series and extract information from multiple sensors.*
- (2) An **automatic characterization method to calculate neural architecture execution latencies for microcontrollers based on a lookup table**, showing that *the number of flops in a neural network architecture is not a suitable proxy metric for its execution latency*, achieving an average error of $\approx \pm 15.57$ ms compared to $\approx \pm 1.59$ ms when calculating the latency of NN architectures using a lookup table approach.
- (3) An **experimental evaluation of MicroNAS based on two state-of-the-art benchmark datasets (UCI-HAR and SkodaR) and two microcontrollers (Nucleo-L552ZE-Q and Nucleo-F446RE)**, showing that:
 - (a) *the proposed search algorithm outperforms a DARTS-based baseline;*
 - (b) *Architectures found by MicroNAS achieve performance comparable to state-of-the-art models running on desktop computers;*
 - (c) *users can configure upper limits for memory and latency constraints, making a trade-off between latency vs. performance and memory vs. performance.*

2 BACKGROUND AND RELATED WORK

In this paper, we tackle the problem of time-series classification on microcontrollers which allows for applications such as predictive maintenance or human activity recognition. In subsection 2.1, we briefly summarize common time-series classification systems. Subsection 2.2 describes related works on hardware aware neural architecture search. MicroNAS builds upon previous knowledge of both topics to solve the time-series classification problem on hardware-constrained microcontrollers.

2.1 Time Series Classification

In the recent past, a common time series classification approach was to use the Nearest Neighbor Classifier coupled with a distance metric such as Dynamic Time Warping (DTW) [6, 24]. Improvements on this approach were made by using ensembles of classifiers with different distance metrics which has lead to systems like HIVE-COTE [25] that consists of 37 individual classifiers. As an alternative, neural networks can be utilized for the time series classification task. Approaches such as InceptionTime [16] and Cui et al. [12] feature CNN based architectures to aggregate temporal information on multiple scales. Other options include the use of RNNs or hybrid models consisting of both CNN and RNN layers [28, 31]. Due to computational complexity, using such systems on MCUs is not feasible, and therefore, neural networks especially designed for the time-series classification task on microcontrollers must be designed. Inspired by the existing CNN system architectures, we develop our NAS search space. This space features searchable cells that are tailored for MCUs and, at the same time, can represent typical structures found in CNN time series classification.

2.2 Neural Architecture Search

Early neural architecture search systems (NAS) [44] formulate the search as a reinforcement learning problem. While this approach produces novel, well-performing architectures, architecture search takes long as in each iteration of the used REINFORCE-algorithm, a neural network has to be trained to convergence and no weight sharing between architectures is employed. To overcome this issue, super-networks as search spaces have been introduced, in which architectures to be found are subgraphs and therefore share their weights [27, 32]. Brock et al. [8] and Pham et al. [32] show, that training this single super-network is enough to emulate any architecture in the search space. Liu et al. extend on this idea, by introducing Differentiable Neural Architecture Search (DNAS) [27]. DNAS utilizes a relaxation schema to make the search continuous, differentiable and, therefore, more resource efficient. In DNAS, the search space is also defined by a super-network, in which a layer has not one but multiple operations. The layer output l is then computed as a convex combination of the output of the operations o scaled by the architectural weights α : $l = \sum_i o_i * \alpha_i$. During architecture search, the regular neural network weights and the architectural weights are jointly optimized using gradient descent. This allows for a structured and therefore more efficient search. After training is complete, the architectural weights represent the found architecture by only selecting the operation from each layer associated with the largest architectural weight while all other operations are discarded. Due to its efficiency, we use DNAS as the basis for the search algorithm in MicroNAS.

Recently, NAS has been extended to be hardware aware (HW-NAS). Systems in this category not only optimize for classical performance metrics such as accuracy or precision but also for hardware specific metrics such as execution latency, peak memory consumption or energy consumption [7]. Optimizing the hardware utilization is especially important when targeting microcontrollers as these devices are typically severely resource constraint. For the peak memory consumption, analytical estimation can be used for precise calculation. In contrast, for the execution latency,

many approaches exist [7]. Real-time latency measurements on the target hardware during architecture search provide precise measurements but prolongs the search drastically [7]. Another common and much faster approach is to use the number of flops or similar metrics as a proxy for the execution latency [22, 40, 42]. While the authors of MicroNets [42] and μ Nas [22] claim the number of operations in a model to be a good proxy for the execution latency when targeting MCUs, Lai et al. [21] argue that this is not the case. A middle ground between the slow but precise on-device measurements during search and the fast but imprecise latency estimations using the number of operations, are lookup tables [7]. With the lookup table approach, operations in the search space are executed before search and the latency measurements of each operator can then be used by the search algorithm without much overhead, which is why we use this approach in MicroNAS.

Existing NAS approaches that target time series data are concerned with classification [33] and forecasting [10] but do not target MCUs and are not hardware aware. In contrast, HW-NAS systems which target MCUs are not concerned with time-series classification. This underlines the need for a HW-NAS time series classification system that combines the techniques of differentiable neural architecture search and the lookup table based latency estimation approach.

3 SYSTEM OVERVIEW

The system overview of MicroNAS can be seen in Figure 1. The system input, shown with dotted lines, consists of a time series dataset, the microcontroller to use, and user-defined limits on the execution latency and peak memory consumption.

In a first step, lookup tables characterizing the execution latency and peak memory consumption of each operator in the search space are obtained. For the execution latency, the operation is executed on the MCU and the latency is measured. The peak memory consumption can be calculated analytically. This characterization has to be performed for each dataset individually as the dataset influences the input and output shapes of the operators in the search space which therefore influences the hardware utilization.

In the second step, hardware aware neural architecture search is performed. MicroNAS leverages a search algorithm based on DNAS. It aims to find the optimal architecture based on the provided dataset and user-defined limits on the execution latency and peak memory consumption. After a suitable architecture was found, it is extracted from the search space by dropping all operations that do not contribute to the final result. The architecture is then retrained from scratch to maximize classification performance. Finally, the trained neural network is converted to the tf-lite format, using *int_8* quantization.

Output of this system is a deployable neural network in the tf-lite format. This output will adhere to previously defined limits on the execution latency and peak-memory consumption on the target microcontroller. The individual system components are introduced in detail in the following sections.

4 LATENCY & PEAK MEMORY ESTIMATION

For MicroNAS to find architectures which obey user-defined limits on the execution latency and peak-memory consumption, it is necessary to estimate the actual execution latency and peak-memory consumption of individual architectures in the search space. We therefore use a lookup table based approach as shown in subsection 4.1 to estimate the execution latencies of individual architectures in the search space. In subsection 4.1 we then outline how to analytically estimate the peak-memory consumption.

4.1 Latency Characterization

When targeting MCUs with NAS, the literature proposes to use the number of operations, such as the number of multiply-accumulate operations (MACs) or the number of floating-point-operations (FLOPS) in a model as proxy metrics [22, 23, 42]. While this approach has shown not to be viable when targeting GPUs [15], Liberis et al. [22, 23] argue, that MCUs do not utilize performance enhancing features such as caching and therefore, latency estimation using the number of operations would be possible. In contrast, Zhang and Zhou [42] find deviations between predicted and actual latencies when investigating individual layers running on MCUs but claim a linear relationship between the number of operations and their execution latencies for whole architectures. Lai et al. [21] on the other hand report, this not to be the case and argue, the total number of operations and parameters are not sufficient proxy metrics for the execution latency.

4.1.1 Lookup Table for Latency Predictions. The approach of building a lookup table for execution latencies in the search space has already been used for targeting mobile phones [40] and is extended to the microcontroller target platform in the proposed system. To build such a lookup table, it is necessary to define the parameters which describe an operation in the search space as we use these parameters as a key to the lookup table. In MicroNAS, an operation is always considered together with an activation function (possibly the identity function) as the TensorFlow Lite Micro framework [13] fuses operations with subsequent activation functions in some cases. Therefore, the following lists of parameters have been established to estimate the execution latency of an operation on a specific MCU:

- **Conv2D:** stride, padding, activation function, input shape, output shape
- **Add:** input size, output size
- **Global Average Pooling:** input size, output size
- **Softmax:** input size

To build the the lookup, a neural network with only the operation to be characterized is generated, converted to the tflite-format, quantized to the *int_8* data-format and executed on the microcontroller. The execution time is measured with the internal CPU-cycle counter of ARM-Cortex processors which can be easily converted to milliseconds. Input

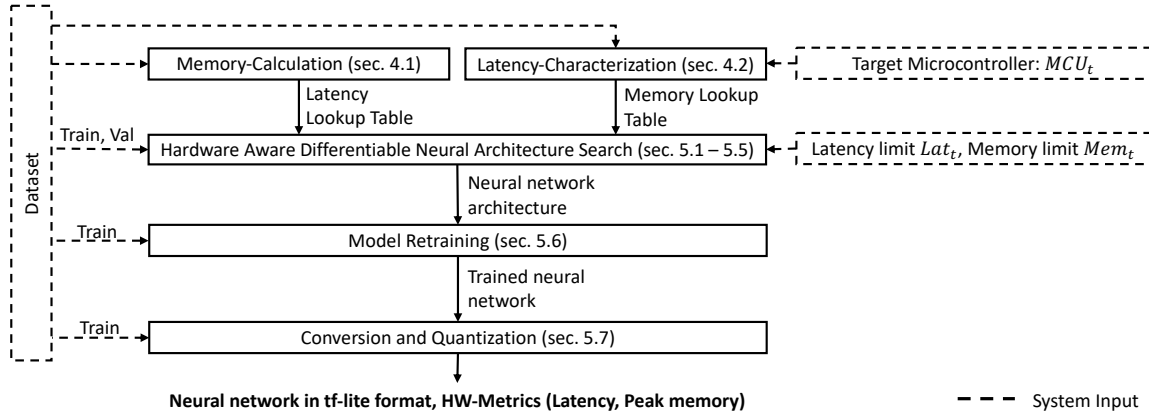
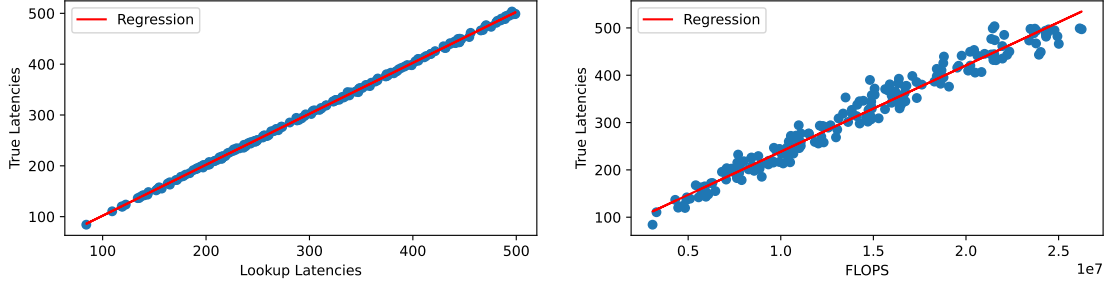


Fig. 1. MicroNAS requires the dataset to be split into three different sets which are used at different stages in the pipeline. The user specifies the dataset to be used, the MCU, MCU_t and the maximum allowed hardware utilization in terms of execution latency (Lat_t) and peak memory consumption (Mem_t). Output of the system is a corresponding neural network in the tf-lite format.



(a) Execution latencies predicted using our lookup table latency estimation (b) Execution latencies predicted using the number of flops as a proxy approach. The mean absolute error is 1.59 ms with an R^2 -score of 99.97. The mean absolute error is 15.57 ms and with an R^2 -score of 96.78.

Fig. 2. Flops vs. execution latency of whole architectures from our search space. Both plots picture the same 201 architectures.

to this characterization system is the search space which depends on the used dataset and the target microcontroller MCU_t . Therefore, the characterization has to be performed for each microcontroller and dataset combination. This process is visualized in figure 3(b)

4.1.2 Latency Prediction Experiment. To conduct our own experiment regarding the execution latency of neural networks on microcontrollers, we randomly draw 200 neural networks from our proposed search space as seen in subsection 5.1. We then execute these architectures on the Nucleo-L552ZE-Q to obtain their true execution latencies but also calculate the number of flops in these architectures. We then plotted the number of flops as well as the prediction using our latency lookup method against the actual execution latencies of the architectures. The results are shown in figure 2. Our lookup table approach achieves an R^2 -score of 99.97 with a mean absolute error of 1.59 ms. The flops based latency estimation achieves an R^2 -score of 96.78 and a mean absolute error of 15.57 ms. Therefore, we can conclude, that the lookup table approach is able to outperform the flops-based latency estimation approach.

In a second experiment, we analyzed the flops-based latency estimation method for predicting the execution latency for individual conv2d-layers. We therefore plotted the flops of all 2D-convolutions in our search space against their true execution latencies. The results can be seen in figure 3(a). The experiment indicated an R^2 -score of 97.57 and a mean absolute error of 5.93 ms. While these results seem promising, the maximum error regarding a single convolutional operation is 72.13 ms. These large errors for single convolutions make the flops-based latency estimation approach unusable for MicroNAS as optimizations are performed on the basis on individual operations.

4.2 Peak Memory Consumption

4.2.1 TFLM memory allocations. When executing a neural network with the TFLM framework [13], memory is needed which is allocated from a user-provided byte array. When minimize the memory footprint of a neural network, the goal is to minimize the size of this byte array. The byte-array is divided into two different parts. The first one is the *Head*-section which contains non-persistent tensor buffers. The minimum required size of the Head-section corresponds to the peak memory usage which is considered in the search by the proposed system. The second one is the *Tail*-section which contains persistent allocations needed to run TFLM. The documentation [38] states that this section contains many random allocations. Due to this randomness, it is not straightforward to calculate the total memory needed for

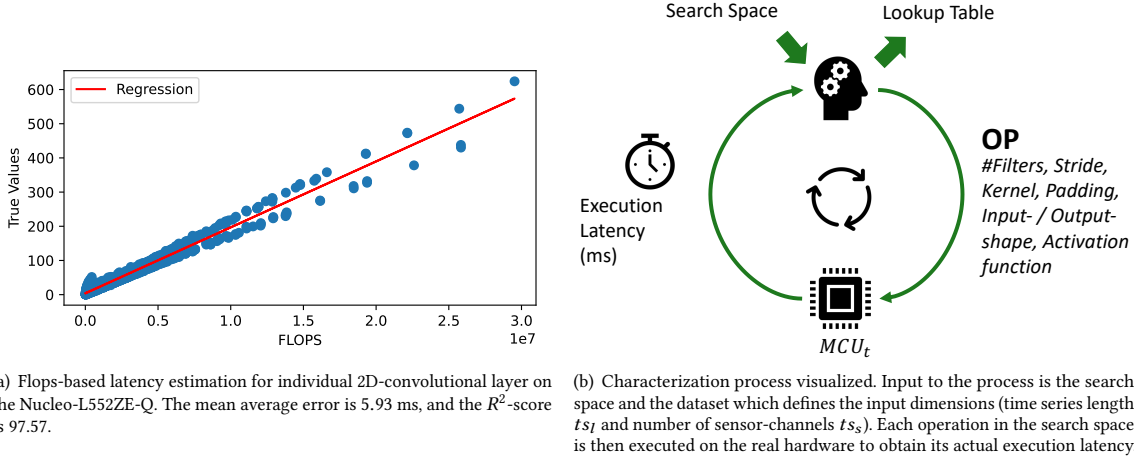


Fig. 3. Left: Flops based latency estimation of 2D-convolutions. Right: Latency characterization process visualized.

execution. Therefore, the proposed system is only concerned with the intermediate tensors during execution and does not take the Tail-section into account when optimizing the peak memory consumption.

4.2.2 Peak memory usage estimation. To calculate the peak memory consumption of an architecture, the literature [7, 42] proposes to use analytical estimation methods which is also the strategy used in this paper. To execute an operation in a neural network, the input and output tensors of the operation need to be present in memory. In addition to that, some operations, e.g. from the CMSIS-NN kernel library [20] require extra memory to perform the computation. When calculating the peak memory of a sequential model without parallel connections, it can be computed as the maximum over the memory requirements of each operation. In general, the required memory to perform an operation can be computed as stated in equation 1.

$$op_{mem}(op) = \sum_i mem(input_i) + mem(output) + extra_mem(op). \quad (1)$$

The function $mem(x)$ calculates the memory required to store a tensor and considers the data format of it. When using *int_8* tensors, only one fourth of the memory is required in comparison to *float_32* tensors. The total memory required to run an operation can then be calculated by summing the memory requirements for the input tensors and the output tensors. On top of that some operations require extra memory to run which is considered in the calculation of the peak memory usage of an architecture [20].

5 MICRONAS - SEARCH SYSTEM

MicroNAS consists of four essential parts which are presented in the following sections. The search space in subsection 5.1 defines the architectures that can be found while the search-algorithm in subsection 5.3 shows how to find a suitable architecture under user-defined execution latency and peak-memory constraints. Subsection 5.4 and subsection 5.5 then show how to deploy found architectures onto microcontrollers.

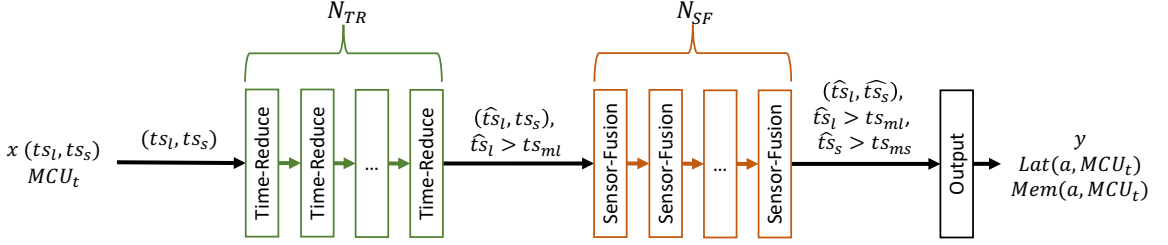


Fig. 4. High-level overview over the search space. The raw, windowed time series x with shape (ts_l, ts_s) is propagated through N_{TR} Time-Reduce and N_{SF} many Sensor-fusion cells. The resulting time series is then of shape (\hat{ts}_l, \hat{ts}_s) . Class probabilities y and hardware metrics are output by the Output cell at the end of the network.

5.1 Search Space

The search space is a Supernet, in which possible architectures are subgraphs. The search space is constructed as a linear stack of cells in which Time-Reduce cells are followed by Sensor-Fusion cells. Both cells are introduced in subsection 5.2. The design rationale for the search space is to first summarize the time series individually using Time-Reduce cells and then allow for cross-channel interaction using the Sensor-Fusion cells. This is a common approach in the domain of time series classification [4, 12, 26, 31, 43]. In the Time-Reduce cells, strided convolutions are used to quickly summarize the time series which reduces computational demand in subsequent cells. As the time series at this stage of the network are the largest, no skip-connections are allowed as fusing the parallel paths would lead to large overheads in both latency and peak memory consumption. After the Time-Reduce cells, the Sensor-Fusion cells enable cross channel interaction and allow combining features at different scales using parallel convolutions with different filter-lengths [12]. Both of these cell types feature learnable architectures. Each Time-Reduce cell and each Sensor-Fusion cell input and output time series data of shape (ts_w, ts_s, c) (time-dimension, sensor-dimension, channels), with $c = 1$ for the first Time-Reduce cell. The output of the last Sensor-Fusion cell is fed into an output cell which converts the time series to class probabilities. In addition to the class probabilities, the search space also outputs hardware metrics, the execution latency $Lat(a, MCU_t)$ and the peak memory consumption $Mem(a, MCU_t)$. These hardware metrics depend on the MCU to use, MCU_t and the architectural weights a indicating the architectural configuration of the search space.

To make the system compatible with a variety of datasets, the macro-architecture of the search space is not fixed but dynamically adapted according to the window-size ts_l and the number of sensor ts_s in the input. The number of Time-Reduce cells can be calculated according to:

$$N_{TR} = \left\lceil \log_2 \left(\frac{ts_l}{ts_{ml}} \right) \right\rceil$$

and the number of Sensor-Fusion cells can be calculated according to:

$$N_{SF} = n_{SF} + sf_{scale} * n_{SF} \quad , \text{with} \quad n_{SF} = \left\lceil \log_2 \left(\frac{ts_s}{ts_{ms}} \right) \right\rceil$$

The parameter sf_{scale} is user-settable to increase the number of Sensor-Fusion cells which allows for deeper networks. The Sensor-Fusion cells can be configured with stride 1 or 2, where the cells added by the sf_{scale} -factor use stride 1 and the rest use stride 2. An overview of this search-space can be seen in figure 4. To improve stability during training, dropout layers with dropout factor 0.3 are used between all cells (not shown in graphic).

To calculate the hardware metrics for the whole search-space, each operation in the search space is aware of its own hardware utilization and therefore not only returns the computed result but also its execution latency and peak memory consumption on MCU_t . This information is then used in the cells to calculate their own hardware utilization. In each searchable cell, architectural weights α exist, which are used to make architectural decision and therefore influence the hardware utilization.

5.1.1 Decision Groups. A decision group α_i is a collection of architectural weights $\alpha_{i,j}$, used to make one-out-of-many decisions. In the scope of this system, it is used to decide how many filters to use in a convolution or which operation to choose at a specific layer in a searchable cell. $\alpha_{i,j}$ denotes the j -th architectural weight in the i -th decision group. During forward propagation, a pseudo probability function is applied to the decision group to weight the different possibilities:

$$\hat{\alpha}_{i,j} = \text{pseudo_prob}(\alpha_{i,j}) \quad (2)$$

After the search, each decision group will be one-hot encoded. This effectively discards all options which are assigned the zero value and therefore the final architecture is determined.

5.1.2 Dynamic Convolutions. A dynamic convolution is a convolution whose number of filters can be searched for efficiently by using weight sharing. In a dynamic convolution, first a convolution with the maximum number of allowed filters f_{max} is applied on the input x . In analogy to FBNetv2 [39], the output of this convolution is then multiplied with a mask to control the number of filters in the output. This mask is the weighted sum of several masks m_i , with architectural weights $\hat{\alpha}_{ch,i} = \text{pseudo_prob}(\alpha_{ch,i})$:

$$y = \text{conv}(x) * \left(\sum_i \hat{\alpha}_{ch,i} * m_i \right)$$

An example overview over this process can be seen in figure 5. As the hardware utilization of a convolution depends on both the number of channels in its input and its output, each dynamic convolution requires the decision groups indicating the number of channels in the input (α_x) and output (α_y). To characterize the latency of a dynamic convolution, regular convolution with all possible combinations of channel configurations must be executed on MCU_t . Therefore, for a dynamic convolution with 64 filters, $64 * 64 = 4096$ characterization steps would be required. To reduce this, the granularity g , with $(f_{max} \bmod g == 0)$ is introduced. It defines the step size when adding or removing filters. This reduces the number of possible combinations from f_{max}^2 to $(f_{max}/g)^2$ which significantly reduces latency characterization cost.

In FBNetv2 [39], effective shape propagation is used to calculate the hardware utilization of such convolutions. This is not possible with our latency lookup table as it only holds discrete latency measurements. Therefore, we calculate the estimated execution latency and memory consumption using interpolation, according to formula 3.

$$\begin{aligned} op_{hw} &= \hat{\alpha}_y^T \cdot HW_{op} \cdot \hat{\alpha}_x \\ &\text{, with} \\ HW_{Conv} &= \begin{bmatrix} HW(g_x, g_y) & \dots & HW(|\alpha_x|g_x, g_y) \\ \vdots & \ddots & \vdots \\ HW(g_1, |\alpha_y| * g_y) & \dots & HW(|\alpha_x|g_x, |\alpha_y|g_y) \end{bmatrix} \end{aligned} \quad (3)$$

When calculating the latency, the $HW(c_1, c_2)$ -function returns the execution latency of the convolution with c_1 many

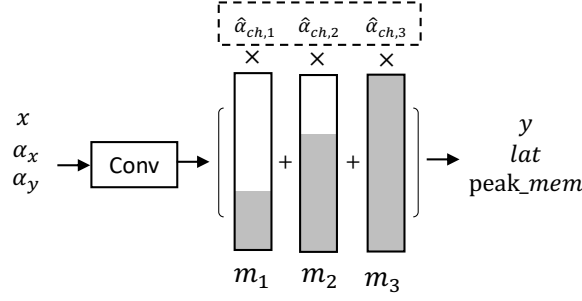


Fig. 5. Dynamic convolution with three different options (e.g. $f_{max} = 24$, $g = 3$) for the number of filters. The binary masks (m_i) zero out certain filters in the output of the convolution. Grey areas are ones and white areas are zeros.

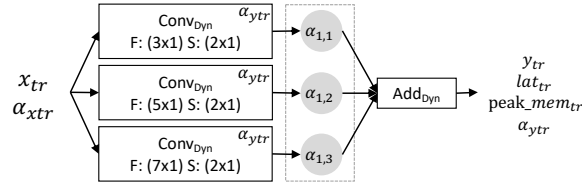


Fig. 6. Time-Reduce cell. Contains two decision groups. α_1 to choose a convolution and α_{ytr} to search for the number of filters. F is the filter size while S is the stride configuration.

channels in the input and c_2 many channels in the output. In analogy, the memory consumption is calculated. In the equation, g_y denotes the granularity corresponding to the output of the convolution while g_x corresponds to the granularity of the input. The same concept can be applied to the Add operations.

5.2 Cells

To accommodate the time series classification task, two types of searchable cells are designed. The Time-Reduce cell aggregates information in the temporal domain while the Sensor-Fusion cell allows for cross channel interaction. After each convolution in the architecture, a ReLU activation function is applied.

5.2.1 Time-Reduce Cell. The Time-Reduce cell shown in figure 6 aggregates local context by applying strided convolutions in the temporal dimension while leaving the sensor-dimension untouched (Filter size: $(\{3, 5, 7\} \times 1)$). This is done to reduce the length of the time series, to save on computational costs in subsequent cells but also to extract and fuse local initial features from the raw data [43]. Two decision groups are used for choosing one of the convolutions (α_1) and the number of filters to be used in the convolution (α_2). The input to this type of cell is a time series x_{tr} of shape (t_{in}, s_{in}, f_{in}) while the output y_{tr} is of shape $(t_{out}, s_{out}, f_{out}) = (0.5 \times t_{in}, s_{in}, f_{in})$. The cell also receives the decision group α_{xtr} which indicates the number of channels in the input x_{tr} . With the output, the cell also propagates the decision group α_{ytr} to indicate how many filters are currently used in it. In addition to that, the layer also propagates its hardware utilization lat_{tr} and $peak_mem_{tr}$.

5.2.2 Sensor-Fusion Cell. A common problem when dealing with time series data is the interaction between the different sensors [6, 43]. To tackle this problem, the Sensor-Fusion cell, seen in figure 7 was designed. The design was inspired by the architecture of InceptionTime [16]. Input to the cell is a time series x_{sf} of shape (t_{in}, s_{in}, f_{in}) . The cell

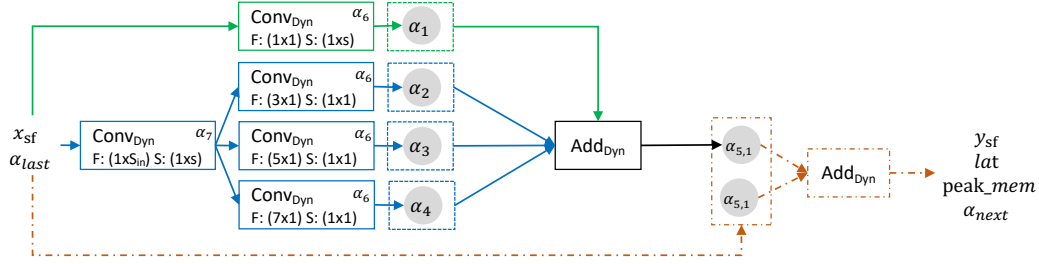


Fig. 7. Sensor-Fusion cell. Consists of three pathways, can be configured with stride one or two and depending on that contains six or seven decision groups. F denotes the filter size while S denotes the stride configuration. The orange pathway is only active, when $stride_{sf} = 1$.

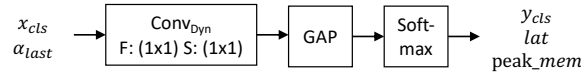


Fig. 8. The output cell features a fixed architecture and is therefore not searchable. First, a dynamic convolution is applied to deal with the different number of channels in x_{cls} . The dimensions of the tensor are reduced by using global average pooling and finally the class probabilities are output using the Softmax operation.

can be configured with stride $stride_{sf}$ to be equal to 1 or 2 which influences the output shape to be $(t_{in}, s_{in}/stride_{sf}, f_{in})$. When the stride equals one, three pathways through the layer exist, shown in green, blue and orange. The orange pathway (dashed) is an identity connection which can be used to skip the layer and is only included if the input and output of the layer have the same shape and is therefore omitted when the stride equals 2. In the main pathway through the layer (shown in blue), first, a dynamic convolution with filter size $(1, S_{in})$ is applied to allow cross channel interaction by performing convolution across all sensor-channels. Then, in a next step, multiple convolutions with filter sizes $(f, 1)$, $f \in \{3, 5, 7\}$ are applied. Each of these convolutions can be individually turned on or off by the search algorithm using the decision groups α_2 , α_3 and α_4 . This allows features to be extracted simultaneously at different temporal scales if necessary. In figure 7, these decision groups are drawn with only one weight, although in reality, for each of the three convolutions, a second parallel zero-connection exists as an alternative which allows the individual selection process. In addition, a skip-connection (shown in green) can be added to the layer using α_1 . As all the pathways through the cell must output tensors with the same shape, the dynamic convolutions in the skip-connection and the dynamic convolutions in the main-block share their decision group α_6 to select the number of filters.

5.2.3 Output cell. The output cell as seen in figure 8 has a non-learnable architecture as it should only output the classification result. It consists of a dynamic convolution with only one choice for the number of filters equal to the number of classes. Global average pooling (GAP) is then used over the time and sensor-dimensions which only leaves the number of channels unchanged so that the resulting vector is of the same length as there are classes. Class probabilities y_{cls} are finally output using the Softmax operation.

5.3 Search Algorithm

To search for a suitable architecture in the search space, we utilize DNAS in a hardware-aware fashion. For this, all performance metrics (loss, execution latency, peak memory consumption) must be differentiable with respect to the architectural weights α . This is achieved by modeling the latency and peak memory consumption as continuous

functions of the architectural weights: $Lat(\alpha, MCU_t)$, $Mem(\alpha, MCU_t)$. While the regular neural network weights w are optimized using the cross-entropy loss on the training-dataset, the architectural weights α are optimized using the following loss function:

$$\mathcal{L}(\alpha, w, MCU_t, Lat_t, Mem_t) = loss_{val}(\alpha, w) + loss_{lat}(\alpha, MCU_t, Lat_t) + loss_{mem}(\alpha, MCU_t, Mem_t) \quad (4)$$

In the equation, $loss_{val}$ denotes the cross-entropy loss on the validation dataset which depends on both sets of weights, α and w . $loss_{lat}$ and $loss_{mem}$ describe the losses caused by the hardware utilization based on the current state of the search space α , MCU_t and the target hardware metrics Lat_t and Mem_t . The latency loss is formulated as

$$loss_{lat} = \eta_{lat} \cdot \log\left(\frac{Lat(\alpha, MCU_t)}{Lat_t}\right) \quad (5)$$

and the peak memory loss is formulated as

$$loss_{mem} = \eta_{mem} \cdot \log\left(\frac{Mem(\alpha, MCU_t)}{Mem_t}\right), \quad (6)$$

with

$$\eta_{lat} = \begin{cases} \gamma_{lat}, & \text{if } Lat(a, m) \geq Lat_t \\ 0, & \text{otherwise} \end{cases} \quad \eta_{mem} = \begin{cases} \gamma_{mem}, & \text{if } Mem(a, m) \geq Mem_t \\ 0, & \text{otherwise} \end{cases} \quad (7)$$

Both formulations ensure the loss to be high, when the current search space configuration α has higher execution latency or peak memory consumption than allowed. In addition to that, the scaling factors γ weight the importance of the individual terms in the loss function. To ensure the user-defined limits on execution latency and peak memory consumption are not violated, both γ -parameters have to be selected sufficiently high. The hardware losses are set to zero when the current configuration of the search space is below the corresponding target as seen in 7. Examples for the hardware losses can be seen in figure 13.

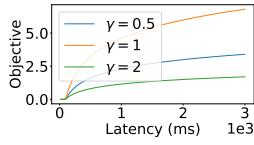


Fig. 9. Execution latency objective with $Lat_t = 100$ ms.

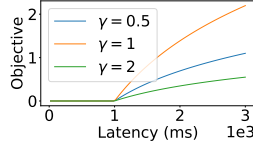


Fig. 10. Execution latency objective with $Lat_t = 1000$ ms.

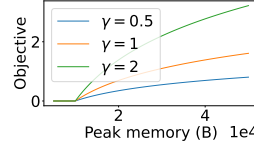


Fig. 11. Peak memory objective with $Mem_t = 10$ kB.

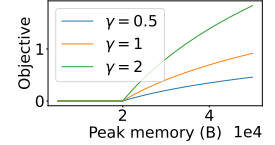


Fig. 12. Peak memory objective with $Mem_t = 20$ kB.

Fig. 13. $loss_{mem}$ plotted for different targets with different values for γ_{lat} and γ_{mem} . The x-axis shows the current estimation of the respective hardware metric.

5.3.1 Optimization Algorithm. To approximate the optimization of equation 4, an iterative update procedure is applied which updates the architectural weights α and the regular neural network weights w iteratively. During the search, for the *pseudo_prob* function in the decision groups, the Gumbel-Softmax [17] with temperature τ is used:

$$y_i = \frac{\exp((\log(\pi_i) + g_i)/\tau)}{\sum_{j=1}^k \exp((\log(\pi_j) + g_j)/\tau)} \quad (8)$$

The Gumbel-Softmax function is a continuous distribution that can be smoothly annealed into a categorical distribution using the temperature parameter τ . When $\tau \rightarrow \infty$, the Gumbel-Softmax distribution approaches a uniform distribution

and when $\tau \rightarrow 0$, the Gumbel-Softmax distribution smoothly approximates the argmax function. When training is started, the architectural weights $\alpha_{i,j}$ in each decision group α_i are randomly initialized uniformly. The search algorithm is executed according to algorithm 1. In an iterative fashion, first the architectural weights α are updated by minimizing the loss shown in Equation 4 on the validation dataset. Then the regular neural network weights w are updated using the regular cross-entropy loss. Both sets of parameters are updated with the Adam optimizer [18]. At the end of each update step, the temperate is updated, so it exponentially decays during the search. The parameter ϵ controls how fast the temperature decreases and lower values for ϵ lead to faster decrease in τ .

Algorithm 1 Search algorithm with learning rates η

```

1: for  $e \leftarrow 1$  to  $Epochs$  do
2:   for  $b \leftarrow 1$  to  $Batches$  do
3:      $\alpha = \alpha - \eta_1 \nabla_{\alpha} \mathcal{L}(\alpha, w, m, Lat_t, Mem_t)$ 
4:      $w = w - \eta_2 \nabla_w \mathcal{L}_{train}(\alpha, w)$ 
5:      $\tau \leftarrow \tau \times \epsilon$ 
6:   end for
7: end for

```

At the beginning of the search, the output of the Gumbel-Softmax is random and all operations in the search space are updated. During search, in each decision group, the most important weight receives the highest value. At the same time τ steadily decreases which leads the Gumbel-Softmax function to approximate a one-hot encoding which leads to one-hot encoded decision-groups at the end of the search. The found architecture is then extracted by removing all operations and filters from the search space that do not contribute to the output. Due to harsh penalties in the loss function when the hardware metrics exceed their limits, the search algorithm finds an architecture that satisfies these limits while the use of the Gumbel-Softmax function with decreasing temperature, forces the algorithm to converge.

5.4 Model Retraining

During architecture search, weight sharing between architectures is applied which allows for an efficient search but at the same time prevents a single architecture to obtain its optimal weights. Therefore, after an architecture has been found, this architecture is trained from scratch to achieve the maximum performance. Training is performed in a quantization aware fashion as we later deploy the resulting model to an MCU using *int_8* quantization.

5.5 Conversion and Quantization

To finally deploy the neural network to the microcontroller we convert the trained network to the tf-lite format. At the same time we quantize it to the *int_8* data format. This greatly reduces computational cost on the microcontroller in terms of execution latency, peak memory consumption and storage requirements with only a minimal loss in classification performance. Further details can be found in append 5.5.1. To then deploy the trained architecture onto the MCU, the TensorFlow Lite Micro Framework (TFLM) [13] is utilized. To speed up computations, the CMSIS-NN [20] neural network kernels provided by ARM are used.

5.5.1 Impact of Post-Training Quantization. Quantization can be used to speed up the computation of a neural network, and it also reduces both the peak memory usage (SRAM) and the amount of storage (Flash) needed. On the other hand, quantization reduces the expressiveness of the network and therefore performance is lost when using quantization. To evaluate how severe this drop of performance is, ten network architectures from the proposed search space are utilized.

Table 1. Overview of tested models in terms of model size and hardware metrics for quantized and non-quantized versions.

Model	Model size non-quant (B)	Model size quant (B)	Model size reduction	Latency non-quant (ms)	Latency quant (ms)	Latency speedup	Peak mem non-quant (B)	Peak mem quant (B)	Peak mem reduction
1	143356	47664	3.01	819.98	253.20	3.24	86656	25604	3.38
2	13924	9120	1.53	71.49	32.88	2.17	27248	8724	3.12
3	35604	17216	2.07	197.12	78.24	2.52	40528	12964	3.13
4	75772	28752	2.64	458.01	148.29	3.09	78976	23076	3.42
5	47452	19984	2.37	236.66	86.90	2.72	40576	12772	3.18
6	186084	58904	3.16	1106.24	326.87	3.38	78976	24612	3.21
7	110076	38192	2.88	568.74	184.13	3.09	78976	23332	3.38
8	261252	82184	3.18	1564.90	490.85	3.19	140992	40548	3.48
9	27836	13352	2.08	156.55	53.87	2.91	40048	12244	3.27
10	56180	23824	2.36	333.70	113.98	2.93	55888	17156	3.26

Table 2. Overview over the classification performance for both the non-quantized and the quantized version of the networks.

Model	Accuracy non-quant (%)	Accuracy quant (%)	Accuracy drop	F1-Score non quant (%)	F1-Score - quant (%)	F1-Score - drop
1	96.94	95.48	1.46	96.09	94.44	1.65
2	88.86	88.86	0.00	84.71	85.13	-0.42
3	93.48	93.48	0.00	90.86	91.09	-0.24
4	95.66	94.58	1.08	93.77	91.81	1.96
5	92.27	91.77	0.50	88.18	87.73	0.45
6	96.98	95.99	0.99	96.08	94.73	1.35
7	96.31	95.03	1.28	95.01	93.05	1.96
8	97.35	96.33	1.02	96.46	95.30	1.16
9	92.47	92.23	0.24	90.35	90.31	0.04
10	94.30	93.92	0.38	91.94	91.34	0.60
11	93.16	91.55	1.61	90.06	87.94	2.13

The architectures were then trained on the SkodaR dataset [35] in a quantization-aware fashion to minimize a decrease in performance. The training dataset was used to set the scale and the zero-point for the quantization to the *int_8* data format [2]. Both the non-quantized version and the quantized versions of the networks were evaluated on the testing dataset.

Table 1 provides an overview over the models under test, while Table 2 shows how performance decreases when using quantization. On average, quantization reduces the model size by a factor of 1.53. For the execution latency, the speedup was at least two times with an average speedup over the five models of 2.90. For the peak memory usage, the reduction on average was 3.28. On average, the accuracy dropped by 0.78% while the F1-Score on average dropped by 0.97%. These results indicate, that quantization, as expected, does impact classification performance negatively but at the same time, hardware metrics improve drastically. For these reasons, the relatively small decrease in classification performance can be accepted.

6 EVALUATION

To showcase MicroNAS, we utilize two established benchmark datasets from the field of human activity recognition. The UCI-HAR dataset [35] is configured with a window size of 128 data-points and features nine sensor channels. It was recorded with a sampling rate of 50 Hz and features six daily activities. Activities include walking, walking upstairs, walking downstairs, sitting, standing and laying. The data collection consists of 3-axial linear acceleration and 3-axial angular velocity obtained from a Galaxy S2 Smartphone worn at the wrist of the participant.

The SkodaR dataset [41] features a window size of 64 data points and 30 sensor channels. It contains gestures of car maintenance scenarios. Detecting such activities creates context to personalized devices and systems [36]. In the scenario, the participants were wearing 20 accelerometers, ten on each arm. In total, 46 activities were recorded in the dataset. All accelerometers were sampled in all three spatial dimensions with a sampling rate of 96 Hz. Typically, the dataset is divided into two, one named “SkodaR” which only includes the right arm sensors and the ten right arm related activities, and the other named “SkodaL” which only includes the left arm accelerometers and the ten left arm related activities.

The choice for these datasets was made as they have become well established benchmark-datasets in the field of human-activity recognition and include IMU data which can be obtained from many commodity devices.

Evaluation was performed on the Nucleo-F446RE [1] equipped with an NRF52832 (Single core, ARM Cortex-M4, 180 MHz CPU clock, 512 kB flash, 128 kB SRAM) and the NUCLEO-L552ZE-Q [30] equipped with a STM32L552 (Single core, ARM Cortex-M33, 80 MHz CPU clock, 512 kB flash, 256 kB SRAM).

6.1 Setup

To demonstrate how the system is easy to use even for people with little to no knowledge of machine learning or MCUs, the same hyperparameters were used for all the experiments. The maximum number of filters for the convolutions in the Time-Reduce cells was set to 16 with the granularity g set to four. For the Sensor-Fusion cells, the maximum number of filters was set to 64 while the granularity was set to eight. To configure the search space on a macro-level, ts_{ml} was 16, ts_{ms} was five and sf_{scale} was two. These settings were chosen to balance between the characterization cost to build the latency lookup table and search space flexibility. For the search algorithm, we set ϵ to 0.995, η_{lat} to two and η_{mem} to four. With this setup the search-space for the UCI-HAR dataset contains $\approx 10^{13}$ architecture and $\approx 10^{22}$ for the SkodaR dataset.

6.2 MicroNAS under different Computational Resource Constraints

6.2.1 Latency vs. Performance. This experiment demonstrates the ability of MicroNAS to find architectures under different latency constraints. Therefore, we disable the loss caused by the peak memory consumption, so it does not influence the search. It is expected that the classification performance will increase as latency targets become higher. Performance metrics for found architectures are presented in figure 14 for the UCI-HAR [35] and in figure 15 for the SkodaR dataset [41]. When higher execution latencies are allowed, classification performance increases for both accuracy and F1-score. It can also be seen, that lower target latencies decrease performance more severely on the Nucleo-L552ZE-Q as it is equipped with a weaker CPU, in terms of clock speeds (80 MHz vs. 180 MHz).

6.2.2 Peak Memory vs. Performance. This experiment demonstrates the ability of MicroNAS to find architectures under different peak memory constraints. The loss caused by the execution latency is omitted, so it does not influence the search. The effects of different target latency constraints on the classification performance can be seen in figure 16

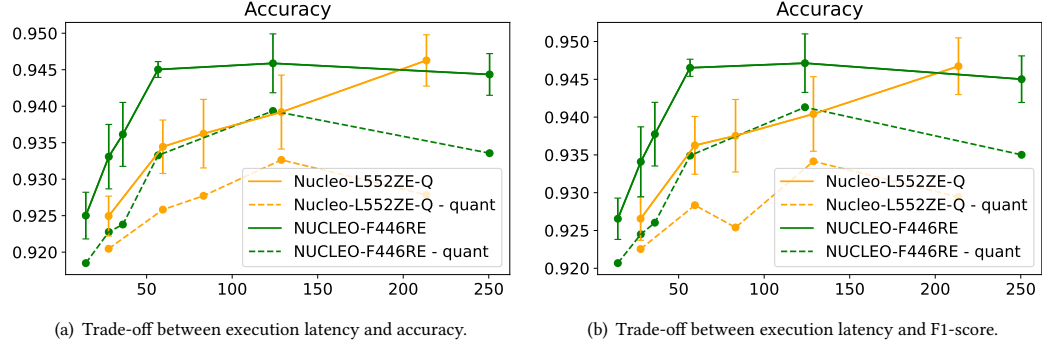


Fig. 14. Comparison on the UCI-HAR dataset.

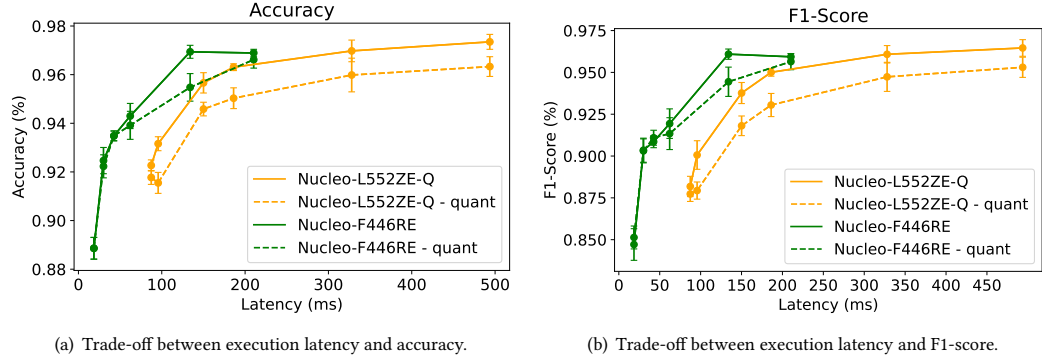


Fig. 15. Comparison on the SkodaR dataset.

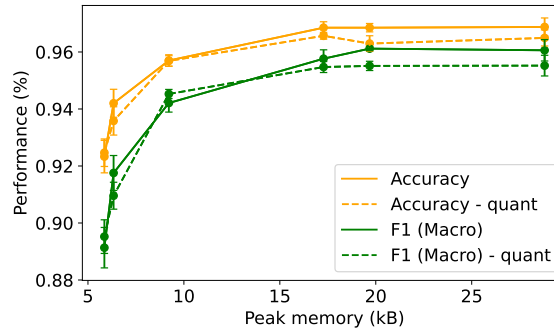


Fig. 16. Trade-off between peak memory consumption and Accuracy / F1-Score (Macro). Comparison on the SkodaR dataset.

for both the classification accuracy and the macro F1-Score. We expect performance to increase as more memory is allowed to be used. As the TFLM-framework [13] is using the same amount of memory on every microcontroller, this experiment is independent of the microcontroller and is therefore only executed on the Nucleo-L552ZE-Q [30].

Table 3. Three architectures found by MicroNAS for the SkodaR dataset compared to SOTA classifiers [28, 31, 43].

Model	MCU	Latency (ms)	Peak memory (B)	Accuracy non-quant (%)	Accuracy quant (%)	F1-Score non-quant (%)	F1-Score quant (%)
MicroNAS 1	Nucleo-F446RE	30.07	21504.0	92.47	92.23	91.40	91.24
MicroNAS 2	Nucleo-L552ZE-Q	150.09	19392.0	95.66	94.58	93.77	92.33
MicroNAS 3	Nucleo-L552ZE-Q	493.69	34560.0	97.35	96.33	96.46	95.30
DARTS softmax	-	-	failed	-	failed	-	-
DARTS gumbel	-	-	96.84	95.04	95.74	93.19	-
DeepConvLSTM	-	-	-	-	98.99	-	-
Mahmud et al.	-	-	-	-	97	-	-

6.3 Comparison to the State-of-the-Art

As there are no other NAS systems which target time series classification on microcontrollers, the network architectures found by MicroNAS are compared against state-of-the art time series classification systems running on desktop computers.

6.3.1 UCI-HAR. Architectures consisting of CNN and GRU layers have been used by Kolkar and Geetha [19] and Dua et al. [14]. Both authors utilize a window size of 2.56 s (same as ours) and achieve classification accuracies of 96.83 % and 96.02 % respectively. In comparison to that, the best performing architecture found for the Nici Sense ME [5] was able to achieve a quantized classification accuracy of 94.34 % when running on the MCU. DARTS [27] coupled with our proposed search space could achieve up to 95.04 % accuracy and 95.59 % F1-Score. The results are summarized in the table 4.

6.3.2 SkodaR. Mahmud et al. [28] utilize the dataset to evaluate their self-attention human activity recognition neural network. The data was downsampled to about 30 Hz and a window length of 1.5 s was used. The self-attention network was able to achieve a macro F1-score of 97 %. Another system, DeepConvLSTM [31], utilizes the dataset, downsamples it to 30 Hz and achieves an F1-score of 98.99 %. It has to be noted, that this performance metric comes from Zhou et al. [43]. In comparison to these results, the best performing architecture found by MicroNAS achieved an F1-Score of 97.35 % while running on the Nucleo-L552ZE-Q. DARTS [27] coupled with our proposed search space could achieve up to 96.84 % accuracy and 95.74 % F1-Score for the version using the Gumbel-Softmax function while the vanilla DARTS-implementation found an architecture with a disconnected graph and therefore failed. The results are summarized in table 3

Table 4. Three architectures found by MicroNAS for the UCI-HAR dataset compared to SOTA classifiers [14, 19].

Model	MCU	Latency (ms)	Peak memory (B)	Accuracy non-quant (%)	Accuracy quant (%)	F1-Score non-quant (%)	F1-Score quant (%)
MicroNAS 1	Nucleo-F446RE	14.45	11520.0	90.21	91.85	92.66	92.07
MicroNAS 3	Nucleo-F446RE	123.84	15360.0	94.59	93.93	94.71	94.13
MicroNAS 2	Nucleo-L552ZE-Q	213.57	15360.0	94.63	92.78	94.67	92.94
DARTS softmax	-	-	94.08	92.01	94.28	92.35	
DARTS gumbel	-	-	95.40	92.97	95.59	93.24	
Kolkar et al. [19]	-	-	96.83	-	-	-	
Dua et al. [14]	-	-	96.02	-	96.19	-	

7 DISCUSSION

In comparison to existing systems, MicroNAS is the first to bring time-series classification to microcontrollers using neural architecture search in a hardware aware fashion. As many IoT and wearable devices are equipped with a variety of time-series producing sensors, whose data must be processed, we expect many application scenarios to benefit from our presented methodology. Especially when user data needs to be processed privately, in real-time or a connection to a server in the cloud is not feasible. Empirical assessment on benchmark datasets and microcontrollers validates MicroNAS. It outperforms random search and a DARTS-based baseline. Comparable performance with desktop models is achieved, while users can customize for latency and memory trade-offs. These contributions affirm MicroNAS as an efficient solution for embedded time series classification.

7.1 Limitations and Future Work

Beyond just the neural network architecture, factors such as the sampling rate, window size, and sensor selection also play a role. To create a complete end-to-end time series classification search system for MCUs, the proposed system can be expanded to encompass these parameters in the search space. Incorporating more sophisticated layer types, such as self-attention, could enhance the search system further, though this may necessitate adding specific operators to the TFLM-framework.

8 CONCLUSION

This paper introduced MicroNAS, a first-of-its-kind hardware-aware neural architecture search (HW-NAS) system specifically designed for time series classification on resource constraint microcontrollers. By utilizing two type of searchable cells, MicroNAS can be used for various datasets which differ in the window-length and the number of sensors. This, coupled with the possibility to set limits on the execution latency and peak memory consumption makes the system usable in various application scenarios such as wearables or real-time systems. This ability of the system to be used in real-time systems is further underlined by our lookup table based latency prediction approach which allows to precisely calculate the execution latency of whole architectures. Our experimental results indicate, that for a variety of different hardware limits, MicroNAS is able to find a suitable neural network architecture.

REFERENCES

- [1] [n. d.]. NUCLEO-F446RE - STM32 Nucleo-64 development board with STM32F446RE MCU, supports Arduino and ST morpho connectivity - STMicroelectronics. <https://www.st.com/en/evaluation-tools/nucleo-f446re.html>. (Accessed on 08/14/2023).
- [2] . 2022. Post-training quantization, TensorFlow Lite. https://www.tensorflow.org/lite/performance/post_training_quantization. (Accessed on 06/17/2022).
- [3] Nasir Abbas, Yan Zhang, Amir Taherkordi, and Tor Skeie. 2018. Mobile Edge Computing: A Survey. *IEEE Internet of Things Journal* 5, 1 (2018), 450–465. <https://doi.org/10.1109/JIOT.2017.2750180>
- [4] Alireza Abedin, Mahsa Ehsanpour, Qinfeng Shi, Hamid Rezaatofghi, and Damith C. Ranasinghe. 2021. Attend and Discriminate: Beyond the State-of-the-Art for Human Activity Recognition Using Wearable Sensors. *Proc. ACM Interact. Mob. Wearable Ubiquitous Technol.* 5, 1, Article 1 (mar 2021), 22 pages. <https://doi.org/10.1145/3448083>
- [5] Arduino. 2022. Arduino Nicla Sense ME. <https://www.bosch-sensortec.com/software-tools/tools/arduino-nicla-sense-me>. (Accessed: 19.05.2022).
- [6] Anthony Bagnall, Jason Lines, Aaron Bostrom, James Large, and Eamonn Keogh. 2017. The great time series classification bake off: a review and experimental evaluation of recent algorithmic advances. *Data Mining and Knowledge Discovery* 31, 3 (01 May 2017), 606–660. <https://doi.org/10.1007/s10618-016-0483-9>
- [7] Hadjer Benmezziane, Kaoutar El Maghraoui, Hamza Ouarnoughi, Smail Niar, Martin Wistuba, and Naigang Wang. 2021. Hardware-Aware Neural Architecture Search: Survey and Taxonomy. In *Proceedings of the Thirtieth International Joint Conference on Artificial Intelligence, IJCAI-21*, Zhi-Hua Zhou (Ed.). International Joint Conferences on Artificial Intelligence Organization, 4322–4329. <https://doi.org/10.24963/ijcai.2021/592> Survey Track.
- [8] Andrew Brock, Theodore Lim, James M. Ritchie, and Nick Weston. 2017. SMASH: One-Shot Model Architecture Search through HyperNetworks. *CoRR* abs/1708.05344 (2017). arXiv:1708.05344 <http://arxiv.org/abs/1708.05344>
- [9] Keyan Cao, Yefan Liu, Gongjie Meng, and Qimeng Sun. 2020. An Overview on Edge Computing Research. *IEEE Access* 8 (2020), 85714–85728. <https://doi.org/10.1109/ACCESS.2020.2991734>
- [10] Donghui Chen, Ling Chen, Zongjiang Shang, Youdong Zhang, Bo Wen, and Chenghu Yang. 2021. Scale-Aware Neural Architecture Search for Multivariate Time Series Forecasting. <https://doi.org/10.48550/ARXIV.2112.07459>
- [11] Jiasi Chen and Xukan Ran. 2019. Deep Learning With Edge Computing: A Review. *Proc. IEEE* 107, 8 (2019), 1655–1674. <https://doi.org/10.1109/JPROC.2019.2921977>
- [12] Zhicheng Cui, Wenlin Chen, and Yixin Chen. 2016. Multi-Scale Convolutional Neural Networks for Time Series Classification. <https://doi.org/10.48550/ARXIV.1603.06995>
- [13] Robert David, Jared Duke, Advait Jain, Vijay Janapa Reddi, Nat Jeffries, Jian Li, Nick Kreeger, Ian Nappier, Meghna Natraj, Tiezhen Wang, Pete Warden, and Rocky Rhodes. 2021. TensorFlow Lite Micro: Embedded Machine Learning for TinyML Systems. In *Proceedings of Machine Learning and Systems*, A. Smola, A. Dimakis, and I. Stoica (Eds.), Vol. 3. 800–811. <https://proceedings.mlsys.org/paper/2021/file/d2ddea18f00665ce8623e36bd4e3c7c5-Paper.pdf>
- [14] Nidhi Dua, Shiva Nand Singh, and Vijay Bhaskar Semwal. 2021. Multi-input CNN-GRU based human activity recognition using wearable sensors. *Computing* 103, 7 (01 Jul 2021), 1461–1478. <https://doi.org/10.1007/s00607-021-00928-8>
- [15] Łukasz Dudziak, Thomas Chau, Mohamed S. Abdelfattah, Royson Lee, Hyeji Kim, and Nicholas D. Lane. 2020. BRP-NAS: Prediction-Based NAS Using GCNs. In *Proceedings of the 34th International Conference on Neural Information Processing Systems (Vancouver, BC, Canada) (NIPS'20)*. Curran Associates Inc., Red Hook, NY, USA, Article 879, 11 pages.
- [16] Hassan Ismail Fawaz, Benjamin Lucas, Germain Forestier, Charlotte Pelletier, Daniel F. Schmidt, Jonathan Weber, Geoffrey I. Webb, Lhassane Idoumghar, Pierre-Alain Muller, and François Petitjean. 2020. InceptionTime: Finding AlexNet for time series classification. *Data Mining and Knowledge Discovery* 34, 6 (01 Nov 2020), 1936–1962. <https://doi.org/10.1007/s10618-020-00710-y>
- [17] Eric Jang, Shixiang Gu, and Ben Poole. 2017. Categorical Reparameterization with Gumbel-Softmax. In *5th International Conference on Learning Representations, ICLR 2017, Toulon, France, April 24-26, 2017, Conference Track Proceedings*. OpenReview.net. <https://openreview.net/forum?id=rkE3y85ee>
- [18] Diederik Kingma and Jimmy Ba. 2014. Adam: A Method for Stochastic Optimization. *International Conference on Learning Representations* (12 2014).
- [19] Ranjit Kolkar and V. Geetha. 2021. Human Activity Recognition in Smart Home using Deep Learning Techniques. In *2021 13th International Conference on Information & Communication Technology and System (ICTS)*. 230–234. <https://doi.org/10.1109/ICTS52701.2021.9609044>
- [20] Liangzhen Lai, Naveen Suda, and Vikas Chandra. 2018. CMSIS-NN: Efficient Neural Network Kernels for Arm Cortex-M CPUs. <https://doi.org/10.48550/ARXIV.1801.06601>
- [21] Liangzhen Lai, Naveen Suda, and Vikas Chandra. 2018. Not All Ops Are Created Equal! <https://doi.org/10.48550/ARXIV.1801.04326>
- [22] Edgar Liberis, Łukasz Dudziak, and Nicholas D. Lane. 2021. μ NAS: Constrained Neural Architecture Search for Microcontrollers. In *Proceedings of the 1st Workshop on Machine Learning and Systems (Online, United Kingdom) (EuroMLSys '21)*. Association for Computing Machinery, New York, NY, USA, 70–79. <https://doi.org/10.1145/3437984.3458836>
- [23] Edgar Liberis and Nicholas D. Lane. 2023. Differentiable Neural Network Pruning to Enable Smart Applications on Microcontrollers. *Proc. ACM Interact. Mob. Wearable Ubiquitous Technol.* 6, 4, Article 171 (jan 2023), 19 pages. <https://doi.org/10.1145/3569468>
- [24] Jason Lines and Anthony Bagnall. 2015. Time series classification with ensembles of elastic distance measures. *Data Mining and Knowledge Discovery* 29, 3 (01 May 2015), 565–592. <https://doi.org/10.1007/s10618-014-0361-2>

- [25] Jason Lines, Sarah Taylor, and Anthony Bagnall. 2016. HIVE-COTE: The Hierarchical Vote Collective of Transformation-Based Ensembles for Time Series Classification. In *2016 IEEE 16th International Conference on Data Mining (ICDM)*. 1041–1046. <https://doi.org/10.1109/ICDM.2016.0133>
- [26] Chien-Liang Liu, Wen-Hoar Hsiao, and Yao-Chung Tu. 2019. Time Series Classification With Multivariate Convolutional Neural Network. *IEEE Transactions on Industrial Electronics* 66, 6 (2019), 4788–4797. <https://doi.org/10.1109/TIE.2018.2864702>
- [27] Hanxiao Liu, Karen Simonyan, and Yiming Yang. 2019. DARTS: Differentiable Architecture Search. arXiv:1806.09055 [cs.LG]
- [28] Saif Mahmud, M. T. H. Tonmoy, Kishor Kumar Bhaumik, A. M. Rahman, M. A. Amin, M. Shoyaib, Muhammad Asif Hossain Khan, and A. Ali. 2020. Human Activity Recognition from Wearable Sensor Data Using Self-Attention. In *ECAI 2020 - 24th European Conference on Artificial Intelligence, 29 August-8 September 2020, Santiago de Compostela, Spain*.
- [29] Hector Mendoza, Aaron Klein, Matthias Feurer, Jost Tobias Springenberg, and Frank Hutter. 2016. Towards Automatically-Tuned Neural Networks. In *Proceedings of the Workshop on Automatic Machine Learning (Proceedings of Machine Learning Research, Vol. 64)*, Frank Hutter, Lars Kotthoff, and Joaquin Vanschoren (Eds.). PMLR, New York, New York, USA, 58–65. https://proceedings.mlr.press/v64/mendoza_towards_2016.html
- [30] STMicroelectronics N.V. [n. d.]. NUCLEO-L552ZE-Q - STM32 Nucleo-144 development board. <https://www.st.com/en/evaluation-tools/nucleo-l552ze-q.html>. (Accessed on 05/31/2022).
- [31] Francisco Javier Ordóñez and Daniel Roggen. 2016. Deep Convolutional and LSTM Recurrent Neural Networks for Multimodal Wearable Activity Recognition. *Sensors* 16, 1 (2016). <https://doi.org/10.3390/s16010115>
- [32] Hieu Pham, Melody Guan, Barret Zoph, Quoc Le, and Jeff Dean. 2018. Efficient Neural Architecture Search via Parameters Sharing. In *Proceedings of the 35th International Conference on Machine Learning (Proceedings of Machine Learning Research, Vol. 80)*, Jennifer Dy and Andreas Krause (Eds.). PMLR, 4095–4104. <https://proceedings.mlr.press/v80/pham18a.html>
- [33] Hojjat Rakhshani, Hassan Ismail Fawaz, Lhassane Idoumghar, Germain Forestier, Julien Lepagnot, Jonathan Weber, Mathieu Bréviillers, and Pierre-Alain Muller. 2020. Neural Architecture Search for Time Series Classification. In *2020 International Joint Conference on Neural Networks (IJCNN)*. 1–8. <https://doi.org/10.1109/IJCNN48605.2020.9206721>
- [34] Nafiul Rashid, Berken Utku Demirel, and Mohammad Abdullah Al Faruque. 2022. AHAR: Adaptive CNN for Energy-Efficient Human Activity Recognition in Low-Power Edge Devices. *IEEE Internet of Things Journal* 9, 15 (2022), 13041–13051. <https://doi.org/10.1109/IJOT.2022.3140465>
- [35] Jorge-L. Reyes-Ortiz, Luca Oneto, Albert Samà, Xavier Parra, and Davide Anguita. 2016. Transition-Aware Human Activity Recognition Using Smartphones. *Neurocomputing* 171 (2016), 754–767. <https://doi.org/10.1016/j.neucom.2015.07.085>
- [36] Albrecht Schmidt, Michael Beigl, and Hans-W Gellersen. 1999. There is more to context than location. *Computers & Graphics* 23, 6 (1999), 893–901. [https://doi.org/10.1016/S0097-8493\(99\)00120-X](https://doi.org/10.1016/S0097-8493(99)00120-X)
- [37] Deepti Sehrawat and Nasib Singh Gill. 2019. Smart Sensors: Analysis of Different Types of IoT Sensors. In *2019 3rd International Conference on Trends in Electronics and Informatics (ICOEI)*. 523–528. <https://doi.org/10.1109/ICOEI.2019.8862778>
- [38] Tensorflow. 2022. tflite-micro/memory_management.md at main · tensorflow/tflite-micro. <https://github.com/tensorflow/tflite-micro/>. (Accessed on 06/12/2022).
- [39] Alvin Wan, Xiaoliang Dai, Peizhao Zhang, Zijian He, Yuandong Tian, Saining Xie, Bichen Wu, Matthew Yu, Tao Xu, Kan Chen, Peter Vajda, and Joseph E. Gonzalez. 2020. FBNetV2: Differentiable Neural Architecture Search for Spatial and Channel Dimensions. In *2020 IEEE/CVF Conference on Computer Vision and Pattern Recognition (CVPR)*. 12962–12971. <https://doi.org/10.1109/CVPR42600.2020.01298>
- [40] Bichen Wu, Xiaoliang Dai, Peizhao Zhang, Yanghan Wang, Fei Sun, Yiming Wu, Yuandong Tian, Peter Vajda, Yangqing Jia, and Kurt Keutzer. 2019. FBNet: Hardware-Aware Efficient ConvNet Design via Differentiable Neural Architecture Search. In *2019 IEEE/CVF Conference on Computer Vision and Pattern Recognition (CVPR)*. 10726–10734. <https://doi.org/10.1109/CVPR.2019.01099>
- [41] Piero Zappi, Daniel Roggen, Elisabetta Farella, Gerhard Troester, and Luca Benini. 2012. Network-Level Power-Performance Trade-Off in Wearable Activity Recognition: A Dynamic Sensor Selection Approach. *ACM Transactions on Embedded Computing Systems* 11 (09 2012), 68:1–68:30. <https://doi.org/10.1145/2345770.2345781>
- [42] Shuai Zhang and Xichuan Zhou. 2021. MicroNet: Realizing Micro Neural Network via Binarizing GhostNet. In *2021 6th International Conference on Intelligent Computing and Signal Processing (ICSP)*. 1340–1343. <https://doi.org/10.1109/ICSP51882.2021.9408972>
- [43] Yexu Zhou, Haibin Zhao, Yiran Huang, Till Riedel, Michael Hefenbrock, and Michael Beigl. 2022. TinyHAR: A Lightweight Deep Learning Model Designed for Human Activity Recognition. In *Proceedings of the 2022 ACM International Symposium on Wearable Computers* (Cambridge, United Kingdom) (*ISWC '22*). Association for Computing Machinery, New York, NY, USA, 89–93. <https://doi.org/10.1145/3544794.3558467>
- [44] Barret Zoph and Quoc V. Le. 2017. Neural Architecture Search with Reinforcement Learning. arXiv:1611.01578 [cs.LG]

Received 3 February 2023; revised xxxxxxxx; accepted xxxxxxxx